



Deletion of *LCMR1* in alveolar type II cells induces lethal impairment of lung structure and function in adult mice

Yueming Wang^{1,2#}, Chunsun Li^{2#}, Zhen Wu^{2#}, Yu Dai², Lu Liu³, Liangan Chen^{1,2}

¹School of Medicine, Nankai University, Tianjin, China; ²Department of Pulmonary and Critical Care Medicine, Chinese PLA General Hospital, Beijing, China; ³Department of Nutrition, Chinese PLA General Hospital, Beijing, China

Contributions: (I) Conception and design: Y Wang, C Li, Z Wu, L Chen; (II) Administrative support: L Chen; (III) Provision of study materials or patients: Y Dai, L Liu; (IV) Collection and assembly of data: Y Wang, C Li, Z Wu; (V) Data analysis and interpretation: Y Wang, Y Dai, L Liu; (VI) Manuscript writing: All authors; (VII) Final approval of manuscript: All authors.

[#]These authors contributed equally to this work.

Correspondence to: Liangan Chen. School of Medicine, Nankai University, Weijin Road No. 94, Tianjin 300071, China; Department of Pulmonary and Critical Care Medicine, Chinese PLA General Hospital, Fuxing Road No. 28, Beijing 100853, China. Email: lianganchen301@263.net.

Background: Previous studies of lung cancer metastasis-related protein 1 (*LCMR1*) mainly focused on its relationship with cancer. However, the function of *LCMR1* in normal tissues or cells is poorly understood. We aimed to investigate the effects of alveolar type II cell (AT2 cell)-specific *LCMR1* deletion on lung structure and function in adult mice.

Methods: Mice carrying the floxed *LCMR1* allele with exons 2–4 flanked by loxP sites were constructed and then crossed with *Sftpc-CreER^{T2}* mice to obtain *Sftpc-CreER^{T2}; LCMR1^{lox/lox}* for AT2 cell-specific *LCMR1* deletion and *LCMR1^{lox/lox}* mice as littermate control. We observed the body weight change, histopathology, lung wet/dry weight ratio, pulmonary function, and survival of the mice, together with the protein concentration, inflammatory cells, and cytokine levels in bronchoalveolar lavage fluid. We also detected AT2 cell numbers and expression of pulmonary surfactant protein in the lung tissues. The apoptosis of AT2 cells was also assessed.

Results: We found that AT2 cell-specific *LCMR1* deletion caused rapid weight loss and increased mortality in mice. Histopathological analysis revealed damaged lung structure, including inflammatory cell infiltration, alveolar hemorrhage, and edema. The lung wet/dry weight ratio was higher and bronchoalveolar lavage fluid (BALF) analysis revealed elevated protein concentration, inflammatory cell counts, and cytokine levels. Pulmonary function measurement showed increased airway resistance, decreased lung compacity, and compliance. We also found massive AT2 cell loss and altered expression of pulmonary surfactant protein. Deletion of *LCMR1* promoted apoptosis in AT2 cells.

Conclusions: We successfully generated an AT2 cell-specific *LCMR1* conditional knockout mouse model and further revealed the crucial role of *LCMR1* in maintaining AT2 cell homeostasis.

Keywords: Lung cancer metastasis-related protein 1 (*LCMR1*); alveolar type II cell; CRISPR/Cas9; conditional gene knockout

Submitted Dec 21, 2022. Accepted for publication Mar 17, 2023. Published online Mar 24, 2023.

doi: 10.21037/jtd-23-293

View this article at: <https://dx.doi.org/10.21037/jtd-23-293>

Introduction

Lung cancer metastasis-related protein 1 (*LCMR1*) was originally identified by differential display polymerase chain reaction (PCR) between human large cell lung carcinoma

cell lines 95C and 95D by our team in 2002 (Genbank accession number: AY148462) (1). Our previous work showed that *LCMR1* is strongly overexpressed in non-small cell lung cancer and its expression is significantly

associated with the clinical stage of patients (1). In addition, the knockdown of *LCMR1* was reported to induce cell apoptosis in different cancer cells *in vitro* (2-4). *LCMR1* is also known as a subunit of the Mediator complex, called *MED19* (5). The Mediator is an evolutionarily conserved multisubunit protein complex that acts as a critical transcription cofactor conveying information between gene-specific transcription factors and RNA polymerase II general transcription machinery (6,7). The mammalian Mediator comprises up to 30 distinct subunits with unique biological functions (8,9). *LCMR1* is a crucial facilitator of peroxisome proliferator-activated receptor gamma (PPAR γ)-mediated gene expression that is required for adipogenesis and maintenance of white adipose tissue (WAT) mass in mice (10). *LCMR1* also acts as a GATA cofactor and *MED1* interactor in *Drosophila* (11). Additionally, *LCMR1* and *MED26* are synergistic functional targets of the RE1 silencing transcription factor (REST) in the epigenetic silencing of neuronal gene expression in non-neuronal cells (12). However, *LCMR1* is still a relatively poorly characterized gene and the role of *LCMR1* in normal lung tissue remains to be elucidated.

The lung is composed of air-conducting bronchi terminating in air-exchanging alveoli. The alveolar epithelium consists of squamous alveolar type I cells (AT1 cells), which are responsible for gas exchange, and cuboidal alveolar type II cells (AT2 cells), which serve as the only source of pulmonary surfactant, reducing surface tension and preventing lung collapse at end-expiration. AT2 cells

also participate in modulation of immune responses and transportation of ions and fluids. In addition, AT2 cells have been recognized as alveolar stem cells with the capacity for self-renewal and differentiation into AT1 cells during lung homeostasis and injury repair (13,14). Specific subgroups of AT2 cells execute the progenitor role in repairing the alveoli, which preferentially re-enter the cell cycle, self-renew and regenerate mature AT1 and AT2 cells after acute lung injury (15,16). However, damaged or denuded alveolar epithelium often triggers defective or overwhelmed repair processes (17).

In this study, we generated a novel tamoxifen-inducible, AT2 cell-specific *LCMR1* conditional knockout mouse model by breeding mice carrying floxed *LCMR1* alleles with *Sftpc-CreER^{T2}* mice, aiming to investigate the effects of AT2 cell-specific *LCMR1* deletion on lung structure and function in adult mice. We demonstrated that AT2 cell-specific *LCMR1* deletion caused increased weight loss, damaged lung structure, impaired lung function, and reduced survival of mice. The lethal phenotype we observed may result from severe AT2 cell depletion, pulmonary surfactant dysfunction, and alveolar structure destruction. These results indicate that *LCMR1* may play an important role in the maintenance of AT2 cell homeostasis. We present the following article in accordance with the ARRIVE reporting checklist (available at <https://jtd.amegroups.com/article/view/10.21037/jtd-23-293/rc>).

Methods

Mice

Mice carrying the floxed *LCMR1* allele were generated in cooperation with Cyagen Biosciences Inc. (Suzhou, China) by combining CRISPR/Cas9 (clustered regularly interspaced short palindromic repeats/CRISPR-associated protein 9) and the Cre/loxP system. Five exons of the *LCMR1* gene have been identified with the ATG start codon in exon 1 and the TAA stop codon in exon 5. Exons 2–4 were selected as the conditional knockout region. Briefly, to engineer the target vector, homology arms and a conditional knockout region were generated by PCR using bacterial artificial chromosome (BAC) clones RP24-220L15 and RP23-427H11 from the C57BL/6J library as templates. The donor vector containing loxP sites, guide RNAs (gRNA1: TTTAAAGGAATTCCACTCCCTGG; gRNA2: TTCACTGGGTTGTTCTAGGCAGG), and Cas9 messenger RNA (mRNA) were co-injected into fertilized mouse eggs to generate targeted conditional knockout mice.

Highlight box

Key findings

- Deletion of *LCMR1* specifically in AT2 cells results in impaired lung structure and function that is lethal to adult mice, which highlights the importance of *LCMR1* in the maintenance of AT2 cell homeostasis.

What is known and what is new?

- *LCMR1* is related to multiple biological processes in different cancer cells *in vitro*; however, its role in normal tissues and cells has not been fully elucidated.
- *LCMR1* is critical for the maintenance of AT2 cell homeostasis.

What are the implications, and what should change now?

- This is the first reported AT2 cell-specific *LCMR1* conditional knockout mouse model to date, which can provide a valuable reference for investigating the function of *LCMR1* in other tissues or cells.

Potential founders were identified by PCR and Sanger sequencing employing mouse tail DNA (data not shown) and then bred to WT mice. F1 offspring ($LCMR1^{lox/wt}$) were also identified by PCR with specific primers for the 5'-loxP site (F-CACGTAACGGCCACAAGTTCGAG, R-CATGAGGTTAAGGAGAGTTGGGAC) and 3'-loxP site (F-GGTAAGTGGGAGGTCAGAGACATGAG, R-CGAAGTTATGTGCACAGTACTGTGG), respectively, and further confirmed via Sanger sequencing and Southern blot analysis (detailed methods not shown).

$Sftpc-CreER^{T2}$ mice (Jackson Laboratory, Bar Harbor, ME, USA) express a tamoxifen-inducible Cre recombinase controlled by the *Sftpc* promoter, which can mediate the deletion of targeted sequences flanked by the loxP sites specifically in AT2 cells. $LCMR1^{lox/wt}$ mice were mated to $Sftpc-CreER^{T2}$ mice, and the offspring were screened for the presence of floxed *LCMR1* and the $Sftpc-CreER^{T2}$ transgene. The double heterozygous mice were then intercrossed to obtain $Sftpc-CreER^{T2}; LCMR1^{lox/lox}$ mice, which were used as breeding pairs to generate AT2 cell-specific *LCMR1* conditional knockout mice ($Sftpc-CreER^{T2}; LCMR1^{lox/lox}$) and littermate control mice ($LCMR1^{lox/lox}$) for the following phenotype study.

Tamoxifen (20 mg/mL in corn oil; Sigma, T5648, St. Louis, MO, USA) was administered via intraperitoneal injection (50 mg/kg) to 6-week-old mice for 5 consecutive days, after which the $Sftpc-CreER^{T2}; LCMR1^{lox/lox}$ mice were termed $LCMR1^{\Delta AT2}$ mice. The control littermates ($LCMR1^{lox/lox}$) received the same doses of tamoxifen. The day of the last dose of tamoxifen administration was recorded as day 0. The mice were housed in individually ventilated cages with free access to food and water under specific pathogen-free (SPF) conditions. All mice were maintained in the C57BL/6J background. A protocol was prepared before the study without registration. All animal experiments were approved by the Institutional Animal Care Use Committee of Chinese PLA General Hospital (No. 2018-X14-25), in compliance with institutional guidelines for the care and use of animals.

Genotyping

Mouse tail genomic DNA (gDNA) was extracted using the DNA extraction kit (Takara, 9765, Shiga, Japan) according to the manufacturer's protocol. The presence of the two loxP sites and the $Sftpc-CreER^{T2}$ transgene was determined by PCR with primers shown in Table S1. DNA of the sorted AT2

cells from lung tissue was also isolated to confirm *LCMR1* deletion through PCR after tamoxifen administration. PCR was performed in a 50 μ L reaction volume using Premix Taq (TaKaRa, RR902A) on a T100™ Thermal Cycler (Bio-Rad, Hercules, CA, USA), and PCR products were detected by agarose gel electrophoresis and visualized using a Molecular Imager ChemiDoc XR System (Bio-Rad) with Image Lab software, version 3.0 (Bio-Rad). The expected sizes of PCR products were also shown in Table S1.

Histopathological analysis

The lung tissues of the mice were fixed in 4% paraformaldehyde for 24 h at 4 °C, dehydrated in a graded ethanol series, and then embedded in paraffin. The paraffin-embedded block was cut into 5- μ m sections which were then deparaffinized, rehydrated, and stained with hematoxylin and eosin (H&E) reagents (Soonbio, Beijing, China) according to the standard procedure. Collagen fibers in the lung sections were detected by Masson's trichrome staining and Sirius red staining using standard procedures. The stained lung sections were examined under a light microscope (Olympus, Tokyo, Japan).

Immunofluorescence and TUNEL staining

For immunofluorescence staining, the 5- μ m paraffin-embedded sections were deparaffinized and rehydrated, followed by heat-mediated antigen retrieval. The sections were blocked with 3% bovine serum albumin (BSA) for 30 min at room temperature and incubated with primary antibodies overnight at 4 °C including anti-prosurfactant protein C (proSP-C) (Millipore, AB3786, Temecula, CA, USA) and anti- α -smooth muscle actin (α -SMA) (Proteintech, 14395-1-AP, Wuhan, China). The sections were then incubated with a secondary antibody (Cy3-conjugated goat anti-rabbit IgG) for 1 h at room temperature. The nuclei were then stained with 4',6-diamidino-2-phenylindole (DAPI) for 10 min. The apoptosis of AT2 cells within lung sections was analyzed using proSP-C and terminal deoxynucleotidyl transferase-mediated dUTP nick-end labeling (TUNEL) co-staining, along with double immunofluorescence staining for proSP-C and cleaved caspase-3 (Servicebio, GB11532, Wuhan, China). Images were captured using an Olympus IX81 fluorescence microscope and a Nikon Eclipse Ti confocal microscope (Tokyo, Japan).

Transmission electron microscopy

Lung tissues were dissected, minced to approximately 1 mm³ pieces as soon as possible, and fixed overnight at 4 °C using 2.5% glutaraldehyde. The samples were then postfixed with 1% osmium tetroxide in cacodylate buffer, dehydrated in a graded ethanol series, and embedded in epoxy resin. Ultrathin sections (70 nm) were obtained using an Ultracut E ultramicrotome (Leica, Wetzlar, Germany), and stained with uranyl acetate and lead citrate. The sections were subsequently examined under an H-7650 transmission electron microscope (Hitachi, Tokyo, Japan) with an attached image capture software.

Lung dissociation and AT2 cells isolation

Lung dissociation was performed as described previously with simple modification (18). The protease solution used for lung digestion in this study contained Collagenase Type I (450 U/mL; Sigma, C0130), Elastase (4 U/mL; Sigma, E1250), Dispase (5 U/mL; Sigma, D4693), and DNaseI (0.33 U/mL; Roche, 10104159001, Mannheim, Germany) dissolved in Dulbecco's minimal essential medium/F12 (DMEM/F12) (Gibco, 11330021, Grand Island, NY, USA). The whole-lung suspension was blocked with TruStain FcX anti-mouse CD16/CD32 (BioLegend, 101319, San Diego, CA, USA) in the Dulbecco's phosphate buffered saline (D-PBS) buffer with 10% fetal bovine serum (FBS), and then stained with anti-CD31-FITC (eBioscience, 11-0311-81), anti-CD45-FITC (eBioscience, 11-0451-81), and anti-CD326-APC (eBioscience, 17-5791-82). Fluorescence activated cell sorting (FACS) was performed on an SH800S Cell Sorter (Sony, San Jose, CA, USA).

Quantitative RT-PCR

Total RNA was isolated using RNASimple Total RNA Kit (Tiangen, DP451, Beijing, China) according to the manufacturer's instructions. Complementary DNA (cDNA) was synthesized using the PrimeScript RT reagent Kit with a gDNA Eraser (Takara, RR047A). Quantitative RT-PCR (qPCR) was performed in a 20 µL reaction volume using KAPA SYBR FAST Universal (KAPA Biosystems, KK4601, Cape Town, South Africa) on MyiQ2 Two-Color Real-Time PCR Detection System (Bio-Rad, Hercules, CA, USA). Primers used for amplification were listed in [Table S2](#). The relative mRNA expression was assessed using the standard $2^{-\Delta\Delta Ct}$ method normalized by β -actin.

Western blot

The total protein were extracted using Radioimmunoprecipitation Assay (RIPA) lysis buffer supplemented with protease and phosphatase inhibitor cocktails (Applygen, C1055, Beijing, China). Protein concentration was measured with a bicinchoninic acid (BCA) protein assay kit (Applygen, P1511). Protein was separated by SDS-polyacrylamide gel electrophoresis (PAGE) and transferred onto polyvinylidene fluoride (PVDF) membranes (Millipore, Billerica, MA, USA). Immunoblotting was performed using specific antibodies, including anti-MED19 (Invitrogen, PA5-78656, Carlsbad, CA, USA), anti- α -SMA (Proteintech), anti-SP-A (Proteintech, 11850-1-AP), anti-SP-B (Bioss, bs-22341R, Beijing, China), anti-SP-C (Proteintech, 10774-1-AP), anti-SP-D (Proteintech, 11839-1-AP), anti-P53 (CST, 2524S, Danvers, MA, USA), anti-B-cell lymphoma-2 (Bcl-2) (PTM Bio., PTM-5777, Hangzhou, China), anti- β -actin (Proteintech, 20536-1-AP), and anti- α -tubulin (PTM Bio., PTM-5442). The protein bands were visualized with a Chemiluminescent HRP Substrate (Millipore) using an automatic chemiluminescence imaging system (Tanon, Shanghai, China). The band intensity was quantified using ImageJ software, version 1.52 (National Institutes of Health) and normalized to α -tubulin or β -actin.

Analysis of bronchoalveolar lavage fluid

After the mice were anesthetized, their tracheas were cannulated and their lungs were lavaged three times with 1 mL of sterile saline. The recovered bronchoalveolar lavage fluid (BALF) was then centrifuged at 500 g for 10 min at 4 °C. The supernatant was used to measure the total protein concentration using a BCA Protein Assay kit (Applygen) and cytokine levels using a LEGENDplex Mouse Inflammation Panel (BioLegend, 740446). The cell pellet was resuspended to determine the total cell numbers using a hemocytometer. Differential cell counts were determined manually from the cytopins of BALF cell pellets stained with H&E, including neutrophils, macrophages, and lymphocytes.

Lung wet/dry weight ratio

After the mice were anesthetized, the right lung was removed and weighed to obtain the wet weight. Subsequently, the samples were desiccated in an oven at 80 °C for 48 h and re-weighed to determine the dry weight. The lung wet/dry weight ratio was then calculated.

Pulmonary function measurement

Pulmonary function was measured using the AniRes2005 lung function testing system (Bestlab, Beijing, China). Briefly, the mice were anesthetized, cannulated via tracheotomy, placed into a sealed plethysmograph chamber, and then connected to a computer-controlled, mechanically ventilated system (AniRes2005). Five consecutive measurements were collected for each mouse, and the average value was used for further analyses of the forced vital capacity (FVC), dynamic lung compliance (C_{dyn}), expiratory resistance (Re), and inspiratory resistance (Ri).

Statistical analysis

Data were exhibited as the mean ± standard error of mean (SEM). Statistical analyses were performed using GraphPad Prism 5.0 software (National Institutes of Health). Comparisons between two groups were processed using the unpaired Student's *t*-test. *P* < 0.05 was considered statistically significant.

Results

Generation of AT2 cell-specific LCMR1 conditional knockout mice

To explore the role of *LCMR1* in lung tissue, we generated a tamoxifen-inducible, AT2 cell-specific *LCMR1* conditional knockout mouse model (*Sftpc-CreER^{T2}; LCMR1^{fllox/fllox}*) for which the gene targeting strategy was briefly illustrated in *Figure 1A*. Initially, we constructed a conditional knockout mouse line with exons 2–4 of the *LCMR1* gene flanked by two loxP sites (*LCMR1^{fllox/wt}*), which was identified and verified by PCR, Sanger sequencing, and Southern blot analysis (*Figure S1A–S1C*). To obtain the *Sftpc-CreER^{T2}; LCMR1^{fllox/fllox}* mice for AT2 cell-specific *LCMR1* deletion, a subsequent breeding scheme was simply depicted in *Figure 1B*. The genotypic distribution of offspring was in accordance with Mendel's law of inheritance (data not shown, only the genotype that we needed for further breeding is listed in the schematic diagram).

We first crossed *LCMR1^{fllox/wt}* mice with *Sftpc-CreER^{T2}* mice to obtain *Sftpc-CreER^{+/+}; LCMR1^{fllox/wt}* mice, which were further bred for *Sftpc-CreER^{+/+}; LCMR1^{fllox/fllox}* mice (*Figure 1C*). Next, the *Sftpc-CreER^{+/+}; LCMR1^{fllox/fllox}* mice were used as breeding pairs to further generate *Sftpc-CreER^{T2}; LCMR1^{fllox/fllox}* mice together with *LCMR1^{fllox/fllox}* mice (*Sftpc-CreER^{T2}* negative) as the littermate control.

Based on Mendel's law of inheritance, the offspring were all expected to harbor the homozygous floxed *LCMR1* allele, and thus, genotyping was performed to detect the presence of the *Sftpc-CreER^{T2}* transgene (*Figure 1D*). Once activated by tamoxifen administration, Cre recombinase can mediate *LCMR1* deletion specifically in the AT2 cells of *Sftpc-CreER^{T2}; LCMR1^{fllox/fllox}*. Six-week-old mice were intraperitoneally injected with tamoxifen for 5 consecutive days, after which *Sftpc-CreER^{T2}; LCMR1^{fllox/fllox}* mice were termed *LCMR1^{ΔAT2}* mice. The DNA of AT2 cells sorted on day 7 was extracted, and *LCMR1* deletion was confirmed by PCR with a 192-bp band detected only in *LCMR1^{ΔAT2}* mice (*Figure 1E*). The analysis of *LCMR1* mRNA expression by qPCR demonstrated a dramatic reduction in the AT2 cells of *LCMR1^{ΔAT2}* mice compared with *LCMR1^{fllox/fllox}* mice (*Figure 1F*). Western blot analysis showed that the *LCMR1* protein expression was also significantly reduced in the AT2 cell of *LCMR1^{ΔAT2}* mice compared with that in *LCMR1^{fllox/fllox}* mice (*Figure 1G*). These results further verified that we successfully generated a tamoxifen-inducible, AT2 cell-specific *LCMR1* conditional knockout mouse model.

Effects of AT2 cell-specific LCMR1 deletion on lung structure and permeability

The histopathology of lungs from *LCMR1^{ΔAT2}* and *LCMR1^{fllox/fllox}* mice was examined to assess the effect of *LCMR1* deletion on lung structure. H&E staining showed prominent structure damage in the lung sections of *LCMR1^{ΔAT2}* mice compared with that in *LCMR1^{fllox/fllox}* mice on day 14 after tamoxifen administration (*Figure 2A*). Specifically, the AT2 cell-specific deletion of *LCMR1* resulted in inflammatory cell infiltration, hemorrhage, edema, and alveolar wall thickening in the lung sections of *LCMR1^{ΔAT2}* mice, which were rarely found in *LCMR1^{fllox/fllox}* mice. There was almost no normal alveolar structure in the areas with severe pathological damage in *LCMR1^{ΔAT2}* mice.

We further examined the ultrastructure of lung tissues through transmission electron microscopy (TEM). Consistent with the histological analysis, the TEM results demonstrated that the alveolar structure was disordered in *LCMR1^{ΔAT2}* mice, while *LCMR1^{fllox/fllox}* mice exhibited a mostly normal structure (*Figure 2B*). The air-blood barrier was thicker in *LCMR1^{ΔAT2}* mice compared with that in *LCMR1^{fllox/fllox}* mice. Additionally, there were dysmorphic or electron-dense lamellar bodies in AT2 cells of *LCMR1^{ΔAT2}* mice compared with that in *LCMR1^{fllox/fllox}* mice.

Sirius red staining of lung sections revealed enhanced

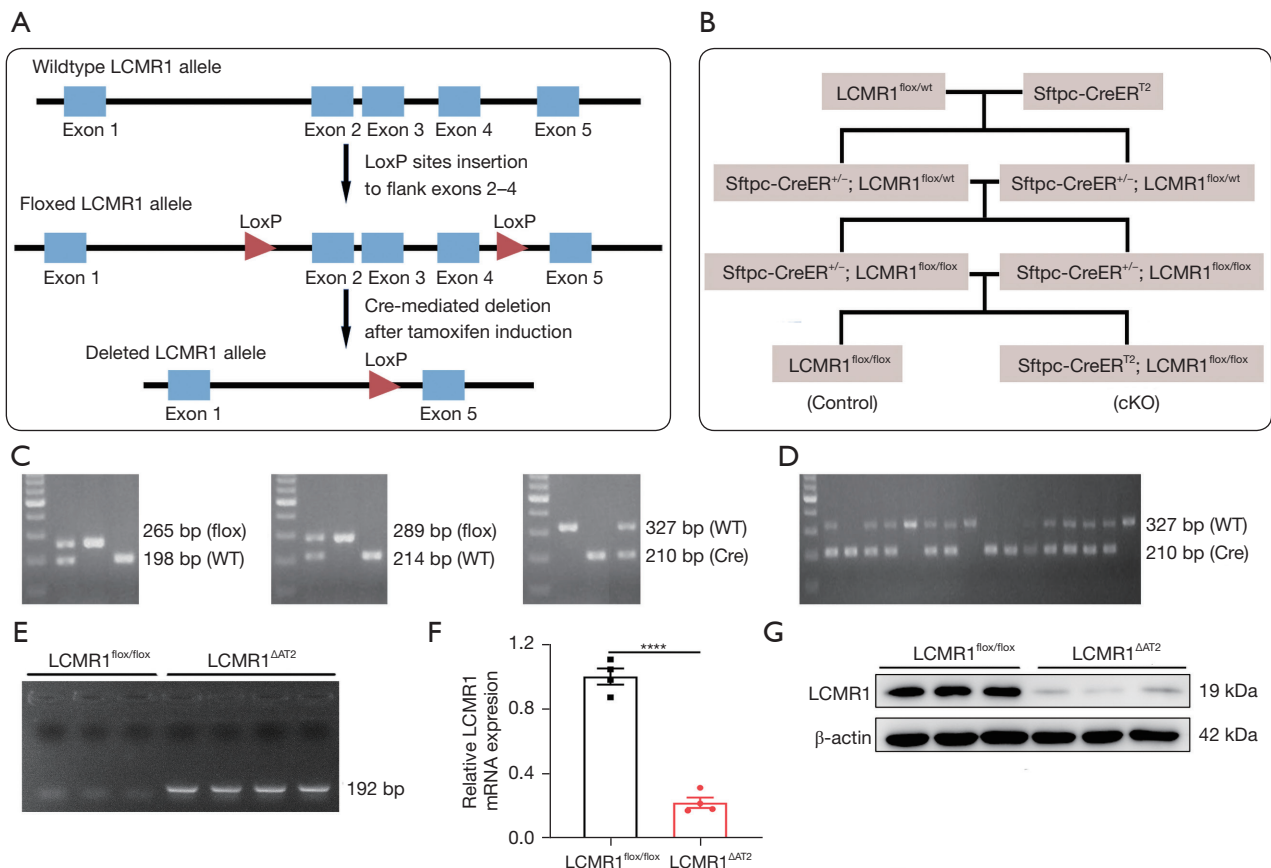


Figure 1 Generation and verification of tamoxifen-inducible, AT2 cell-specific *LCMR1* conditional knockout mice. (A) Schematic diagram of the gene targeting strategy. Mice carrying the floxed *LCMR1* allele in which exons 2–4 were flanked by loxP sites were constructed using CRISPR/Cas9 technology. Cre-mediated excision resulted in the deleted *LCMR1* allele lacking exons 2–4 in AT2 cells after tamoxifen induction. (B) Schematic diagram of the breeding scheme. (C) Genotyping of mice by PCR for the floxed *LCMR1* allele and *Sftpc-CreER*^{T2} transgene to identify *Sftpc-CreER*^{+/-}; *LCMR1*^{flox/flox} mice. The floxed *LCMR1* allele produced 265-bp (left panel) and 289-bp band (middle panel), indicating the two loxP sites respectively, while the wild-type allele produced 198-bp (left panel) and 214-bp band (middle panel), respectively. The expected size of the *Sftpc-CreERT2* transgene was 210 bp (right panel). (D) Genotyping of mice by PCR for the presence of *Sftpc-CreERT2* transgene. (E) Detection of the *LCMR1* deletion band (192 bp) by PCR in AT2 cells sorted on day 7 from *LCMR1*^{flox/flox} (n=3) and *LCMR1*^{ΔAT2} mice (n=4). (F) qPCR analysis of *LCMR1* mRNA expression in AT2 cells sorted on day 7 from *LCMR1*^{flox/flox} and *LCMR1*^{ΔAT2} mice, normalized to β-actin (n=4/group). (G) Western blot analysis of *LCMR1* protein expression in AT2 cells sorted on day 7 from *LCMR1*^{flox/flox} and *LCMR1*^{ΔAT2} mice, normalized to β-actin (n=3/group). Data are presented as the mean ± SEM. ****, P<0.0001 by unpaired Student's *t*-test. AT2, alveolar type II; *LCMR1*, lung cancer metastasis-related protein 1. SEM, standard error of mean; PCR, polymerase chain reaction.

collagen deposition mainly around the bronchioles or adjacent to the pleura in *LCMR1*^{ΔAT2} mice compared with *LCMR1*^{flox/flox} mice (Figure 2C). Collagen deposition was similarly evidenced by Masson's trichrome staining (Figure 2D). Furthermore, we also detected the expression of α-smooth muscle actin-positive (α-SMA), a marker of the myofibroblasts (19). The immunofluorescence staining results showed more α-smooth muscle actin-positive

(α-SMA-positive) cells in the lung sections of *LCMR1*^{ΔAT2} mice compared with those in *LCMR1*^{flox/flox} mice (Figure 2E). Additionally, western blot showed a significant increase in the whole-lung protein expression of α-SMA in *LCMR1*^{ΔAT2} mice compared with that in *LCMR1*^{flox/flox} mice (Figure 2F). Besides the pathological changes, we found that the lung wet/dry weight ratio was significantly higher in *LCMR1*^{ΔAT2} mice than that in *LCMR1*^{flox/flox} mice (Figure 2G),

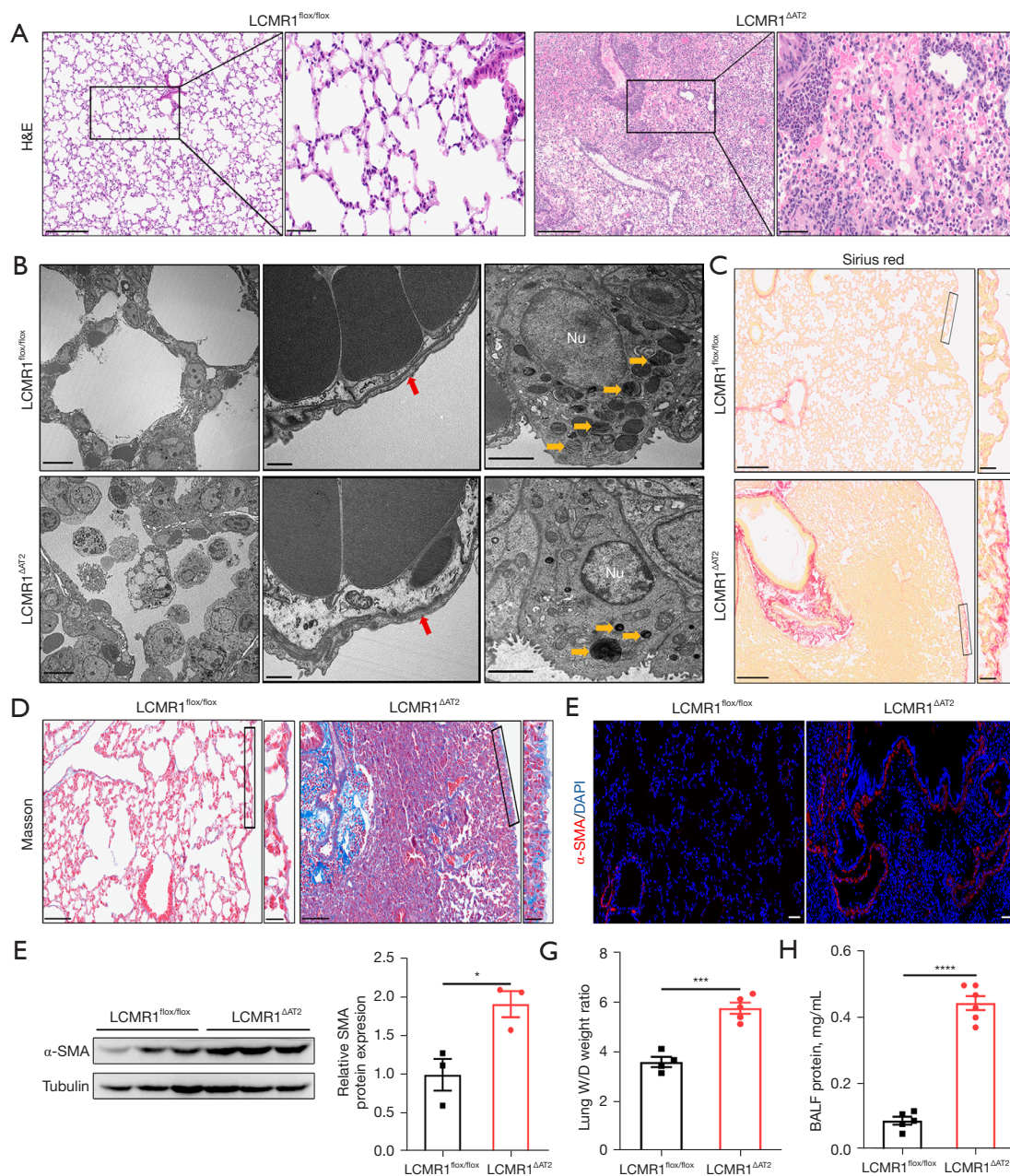


Figure 2 Effects of AT2 cell-specific *LCMR1* deletion on lung structure and permeability. Lung tissues and BALF were collected from *LCMR1*^{flox/flox} and *LCMR1*^{ΔAT2} mice on day 14 after tamoxifen administration. (A) Representative images of H&E-stained lung sections. The insets (left) are shown magnified on the right. Scale bars, 200 μ m (left panels) and 50 μ m (right panels). (B) Representative transmission electron microscopy images of lung sections. Red arrows: air-blood barrier. Yellow arrows: lamellar bodies in AT2 cell. Nu: nucleus. Scale bars, left panels (10 μ m, \times 1,200), right panels (2 μ m, \times 6,800), middle panels (1 μ m, \times 9,300). (C) Representative images of the Sirius red-stained lung sections. The insets (left) are shown magnified on the right. Scale bars, 200 μ m (left panels) and 20 μ m (right panels). (D) Representative images of Masson's trichrome-stained lung sections. The insets (left) are shown magnified on the right. Scale bars, 100 μ m (left panels) and 20 μ m (right panels). (E) Representative images of immunofluorescence staining for α -SMA (red) on lung sections. Nuclei were stained with DAPI (blue). Scale bars, 50 μ m. (F) Western blot analysis of α -SMA protein expression in lung tissues, normalized to α -tubulin (n=3/group). (G) Quantification of lung wet/dry (W/D) weight ratio (n=4–5/group). (H) The concentration of total protein in BALF (n=5–6/group). *, P<0.05, ***, P<0.001, ****, P<0.0001 by unpaired Student's *t*-test. AT2, alveolar type II; *LCMR1*, lung cancer metastasis-related protein 1. H&E, hematoxylin and eosin.

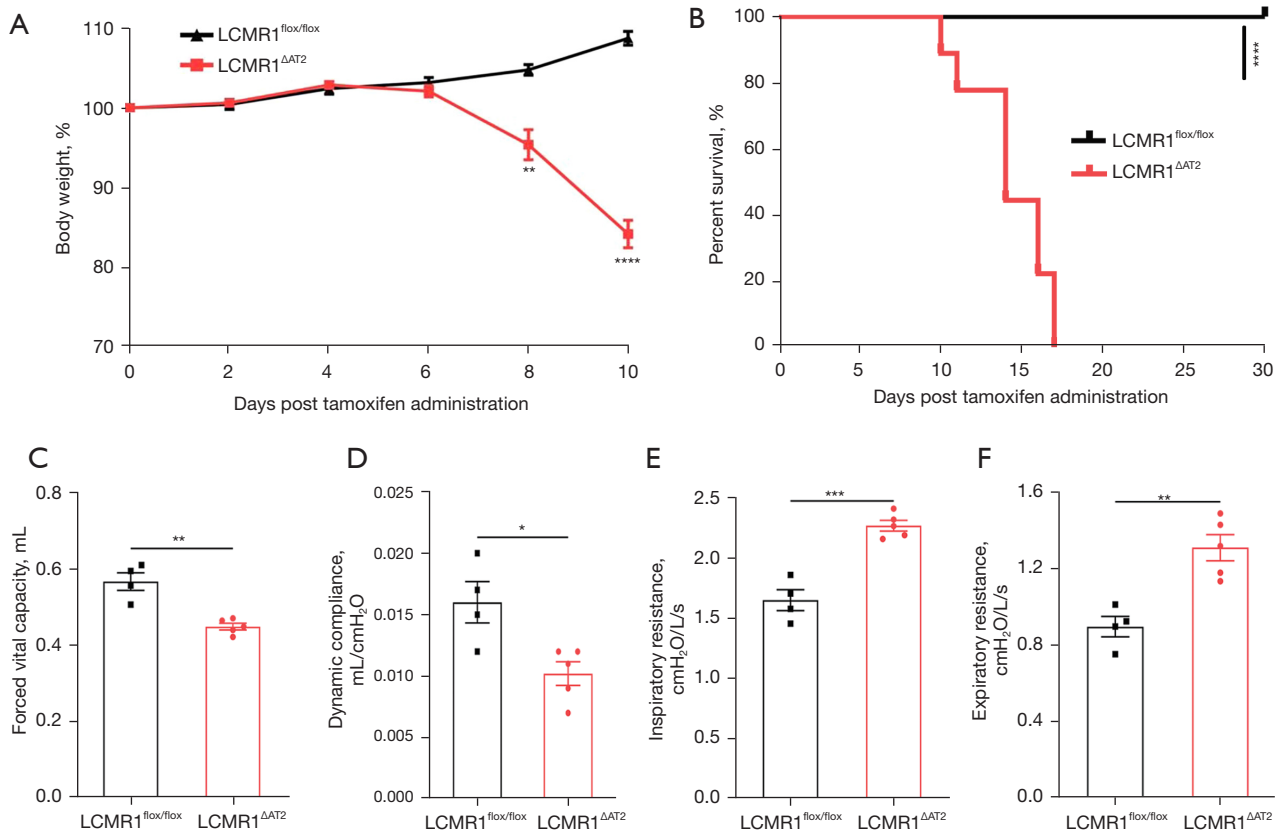


Figure 3 Effects of AT2 cell-specific *LCMR1* deletion on body weight, pulmonary function, and survival. (A) Body weight of *LCMR1*^{flx/flx} and *LCMR1*^{ΔAT2} mice after tamoxifen administration, shown as the percentage of the body weight on day 0 (n=5–7/group). (B) Survival curves of *LCMR1*^{ΔAT2} mice and *LCMR1*^{flx/flx} mice (n=9/group). A log-rank test was used for statistical analysis of the survival curve. (C–F) Analysis of forced vital capacity (C), dynamic compliance (D), inspiratory resistance (E), and expiratory resistance (F) of *LCMR1*^{ΔAT2} mice (n=5) and *LCMR1*^{flx/flx} mice (n=4) on day 14 after tamoxifen administration. Data are expressed as the mean ± SEM. *, P<0.05, **, P<0.01, ***, P<0.001, ****, P<0.0001 by unpaired Student's *t*-test. AT2, alveolar type II; *LCMR1*, lung cancer metastasis-related protein 1.

accompanied by a significant increase in BALF protein concentration collected from *LCMR1*^{ΔAT2} mice compared with that from *LCMR1*^{flx/flx} mice (Figure 2H), which was indicative of higher lung permeability.

Effects of AT2 cell-specific *LCMR1* deletion on body weight, pulmonary function, and survival

We monitored the health status of *LCMR1*^{ΔAT2} mice and *LCMR1*^{flx/flx} mice daily after tamoxifen administration. Data on body weight changes were expressed as a percentage of body weight at day 0 (Figure 3A). *LCMR1*^{ΔAT2} mice exhibited increased body weight loss as early as day 4 after tamoxifen administration, whereas all *LCMR1*^{flx/flx} mice were healthy and continued to gain weight throughout the observation period. There was a significant difference

in the weight change of *LCMR1*^{ΔAT2} mice and *LCMR1*^{flx/flx} mice after day 6, which increased with time. Despite prominent body weight loss, *LCMR1*^{ΔAT2} mice exhibited shortness of breath, a hunched posture, and decreased activity, followed by death. Notably, the *LCMR1*^{ΔAT2} mice showed significantly increased mortality compared with the *LCMR1*^{flx/flx} mice (Figure 3B). The survival of *LCMR1*^{ΔAT2} mice was significantly decreased with the onset of mortality as early as day 10 after tamoxifen administration. There were no surviving *LCMR1*^{ΔAT2} mice after day 17, with a median survival of 14 days post-tamoxifen, whereas all *LCMR1*^{flx/flx} mice were alive and healthy throughout the 30 days observed.

We also examined whether the observed histopathological changes have any effect on lung function through invasive pulmonary function testing. The forced vital capacity

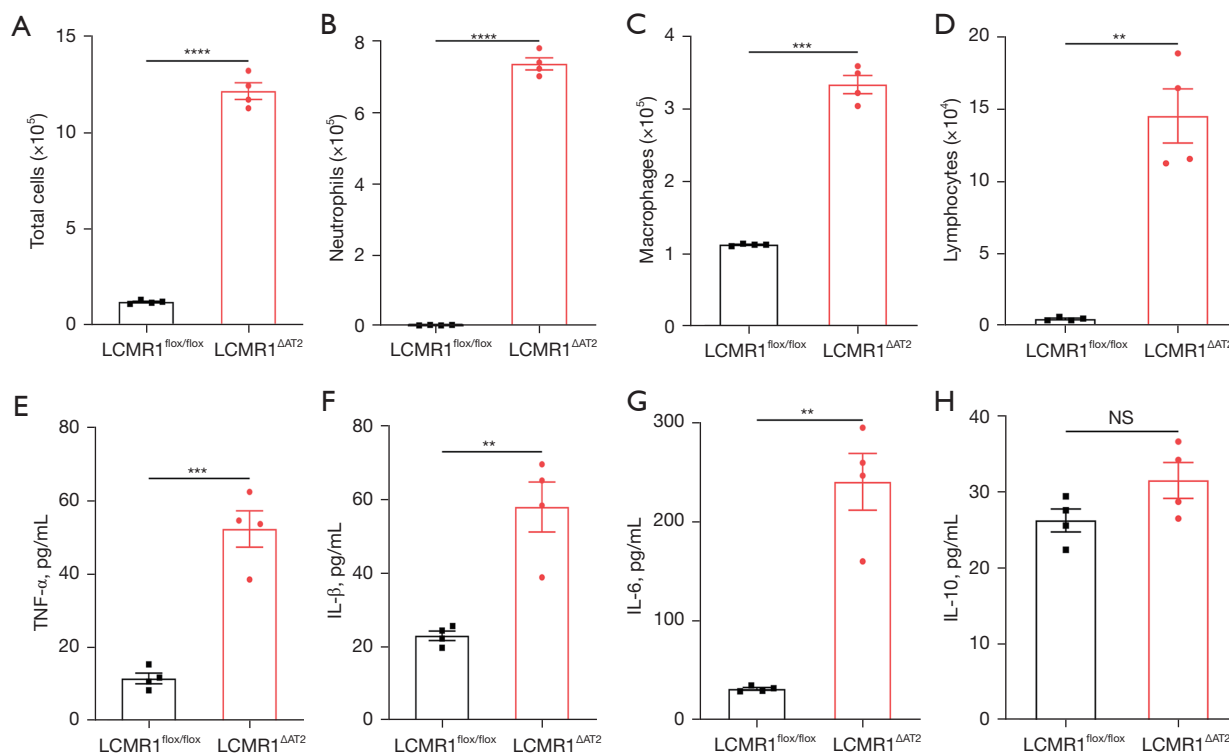


Figure 4 Effect of AT2 cell-specific *LCMR1* deletion on cellularity and inflammatory cytokines in BALF. (A-D) Counts of total cells (A), neutrophils (B), macrophages (C), and lymphocytes (D) in BALF collected from *LCMR1*^{flox/flox} and *LCMR1*^{ΔAT2} mice on day 14 after tamoxifen administration (n=4/group). (E-H) Levels of TNF-α (E), IL-1β (F), IL-6 (G), and IL-10 (H) in BALF collected from *LCMR1*^{flox/flox} and *LCMR1*^{ΔAT2} mice on day 10 after tamoxifen administration (n=4/group). Data are expressed as the mean ± SEM. **, P<0.01, ***, P<0.001, ****, P<0.0001; NS, not significant by unpaired Student's *t*-test. AT2, alveolar type II; *LCMR1*, lung cancer metastasis-related protein 1.

(FVC) was significantly decreased in *LCMR1*^{ΔAT2} mice compared with that in *LCMR1*^{flox/flox} mice (Figure 3C). Additionally, the dynamic compliance (C_{dyn}) was significantly lower in *LCMR1*^{ΔAT2} mice compared with that in *LCMR1*^{flox/flox} mice (Figure 3D). We also found increases in the inspiratory resistance (R_i) and expiratory resistance (R_e) of *LCMR1*^{ΔAT2} mice compared with that of *LCMR1*^{flox/flox} mice (Figure 3E, 3F). These data suggested increased airway resistance and decreased lung compacity and compliance in *LCMR1*^{ΔAT2} mice.

Effects of AT2 cell-specific *LCMR1* deletion on cellularity and inflammatory cytokines in BALF

To evaluate the effect of *LCMR1* deletion on the inflammatory response in the lung, we detected the total cell counts, differential cell counts, and typical cytokine levels in BALF collected from *LCMR1*^{flox/flox} and *LCMR1*^{ΔAT2} mice on day 14 after tamoxifen administration. BALF

from *LCMR1*^{ΔAT2} mice exhibited a substantial increase in total cell counts compared with that from *LCMR1*^{flox/flox} mice (Figure 4A). We further performed differential cell counts, which revealed significantly increased neutrophils from *LCMR1*^{ΔAT2} mice compared with *LCMR1*^{flox/flox} mice (Figure 4B). Similar trends were also observed in the numbers of macrophages and lymphocytes in BALF (Figure 4C, 4D).

Regarding typical cytokines, the concentrations of tumor necrosis factor-α (TNF-α), interleukin-1β (IL-1β), IL-6 and IL-10 were also detected in BALF from *LCMR1*^{flox/flox} and *LCMR1*^{ΔAT2} mice on day 14 after tamoxifen administration. We also observed significantly elevated levels of proinflammatory cytokines in BALF from *LCMR1*^{ΔAT2} mice compared with that from *LCMR1*^{flox/flox} mice, including TNF-α, IL-1β, and IL-6 (Figure 4E-4G). The level of the typical anti-inflammatory cytokine, IL-10, also trended higher in *LCMR1*^{ΔAT2} mice compared with *LCMR1*^{flox/flox} mice but the increase was not significantly different between the two groups (Figure 4H). Alterations

of cell and cytokine profiles in BALF indicated an enhanced inflammatory response in the lungs of *LCMR1*^{ΔAT2} mice, which was consistent with the histological changes.

Effects of *LCMR1* deletion on the AT2 cell number and pulmonary surfactants

Next, we assessed the impact of *LCMR1* on the number and function of AT2 cells. Immunofluorescence staining for the AT2 cell marker proSP-C (20) was performed on lung sections from *LCMR1*^{flox/flox} and *LCMR1*^{ΔAT2} mice on day 14 after tamoxifen administration, which revealed an apparent reduction of proSP-C-positive (proSP-C⁺) cells in *LCMR1*^{ΔAT2} mice compared with that in *LCMR1*^{flox/flox} mice, indicating a loss of AT2 cells (Figure 5A). As AT2 cells synthesize and secrete surfactant proteins, we then analyzed the expressions of *SP-A*, *SP-B*, *SP-C*, and *SP-D* in lung tissue by qPCR and western blot analysis. qPCR analysis showed a significant reduction in the mRNA expressions of *SP-A*, *SP-B*, and *SP-C* in the lung tissues of *LCMR1*^{ΔAT2} mice compared with those of *LCMR1*^{flox/flox} mice, while there was no significant change in whole-lung *SP-D* mRNA expression in *LCMR1*^{ΔAT2} mice compared with that in *LCMR1*^{flox/flox} mice (Figure 5B-5E).

Similarly, western blot analysis revealed decreased protein levels of *SP-A* and *SP-B*, as well as *SP-C* which was nearly undetectable in the lung tissues of *LCMR1*^{ΔAT2} mice compared with that of *LCMR1*^{flox/flox} mice (Figure 5F,5G). On the contrary, the whole-lung *SP-D* protein level was significantly increased in *LCMR1*^{ΔAT2} mice compared with that in *LCMR1*^{flox/flox} mice (Figure 5F,5G). These results indicated that *LCMR1* deficiency led to the loss of AT2 cells and the dysfunction of pulmonary surfactants.

AT2 cell-specific *LCMR1* deletion promotes apoptosis in AT2 cells

Since *LCMR1* knockdown was reported to promote apoptosis in lung cancer cells (2), we hypothesized that apoptosis may also play an important role in the loss of AT2 cells in *LCMR1*^{ΔAT2} mice. To detect AT2 cell apoptosis, we performed double staining for proSP-C and TUNEL on lung sections from *LCMR1*^{flox/flox} and *LCMR1*^{ΔAT2} mice on day 10 after tamoxifen administration (Figure 6A), which showed more proSP-C and TUNEL double positive (proSP-C⁺TUNEL⁺) cells in *LCMR1*^{ΔAT2} mice compared with those in *LCMR1*^{flox/flox} mice. Likewise, double staining for proSP-C and cleaved caspase-3 on lung sections also

showed more apoptotic AT2 cells in *LCMR1*^{ΔAT2} mice than those in *LCMR1*^{flox/flox} mice (Figure 6B). Additionally, elevated apoptosis in AT2 cells was further confirmed by western blot analysis for p53 and Bcl-2 protein expression, which exhibited upregulated p53 expression paralleled by downregulated Bcl-2 expression in AT2 cells from *LCMR1*^{ΔAT2} mice compared with that from *LCMR1*^{flox/flox} mice (Figure 6C-6E).

Discussion

As *LCMR1* was first identified from human large-cell lung carcinoma cell lines, previous studies of *LCMR1* mainly focused on its relationship with cancer, especially regarding cell growth, apoptosis, invasion, and metastasis in different cancer types (2-4,21-25). *LCMR1* down-regulation can induce laryngocarcinoma cancer cell apoptosis via activation of apoptotic protease activating factor 1 (Apaf-1) (4). *LCMR1* can also promote melanoma cell invasion through activating Tetraspanin 8 (Tspan8) protein expression (21). Additionally, *LCMR1* can promote breast cancer progression by regulating the EGFR/MEK/ERK signaling pathway (22). Simultaneously, given its role as a subunit of the Mediator complex, *LCMR1* is also expected to function as a co-activator of RNA polymerase II enzyme to regulate gene transcription in normal tissues and cells, which has rarely been reported. In this study, we generated the first tamoxifen-inducible, AT2 cell-specific *LCMR1* conditional knockout mouse model and preliminarily characterized its phenotype. We found prominent structural abnormalities in the lung tissues of *LCMR1*^{ΔAT2} mice, including inflammatory cell infiltration, collagen deposition, alveolar hemorrhage, and edema. Consistently, we also observed impaired pulmonary function, including increased airway resistance and decreased lung capacity and compliance, in *LCMR1*^{ΔAT2} mice. All *LCMR1*^{ΔAT2} mice died within 17 days after tamoxifen administration. Collectively, these results showed that AT2 cell-specific *LCMR1* deletion could induce lethal lung structure and function alterations in adult mice.

CRISPR/Cas9 gene editing technology can effectively induce precise cleavage at target sites in the genome based on short RNA-guided DNA recognition (26,27). Due to its high efficiency and precision, CRISPR/Cas9 has been used to manipulate genes *in vitro* and *in vivo* to investigate phenotypic changes and underlying mechanisms of respiratory diseases (28,29). CRISPR/Cas9 can also be used for drug screening, target validation and novel target discoveries, especially in lung cancer (30,31). The Cre/

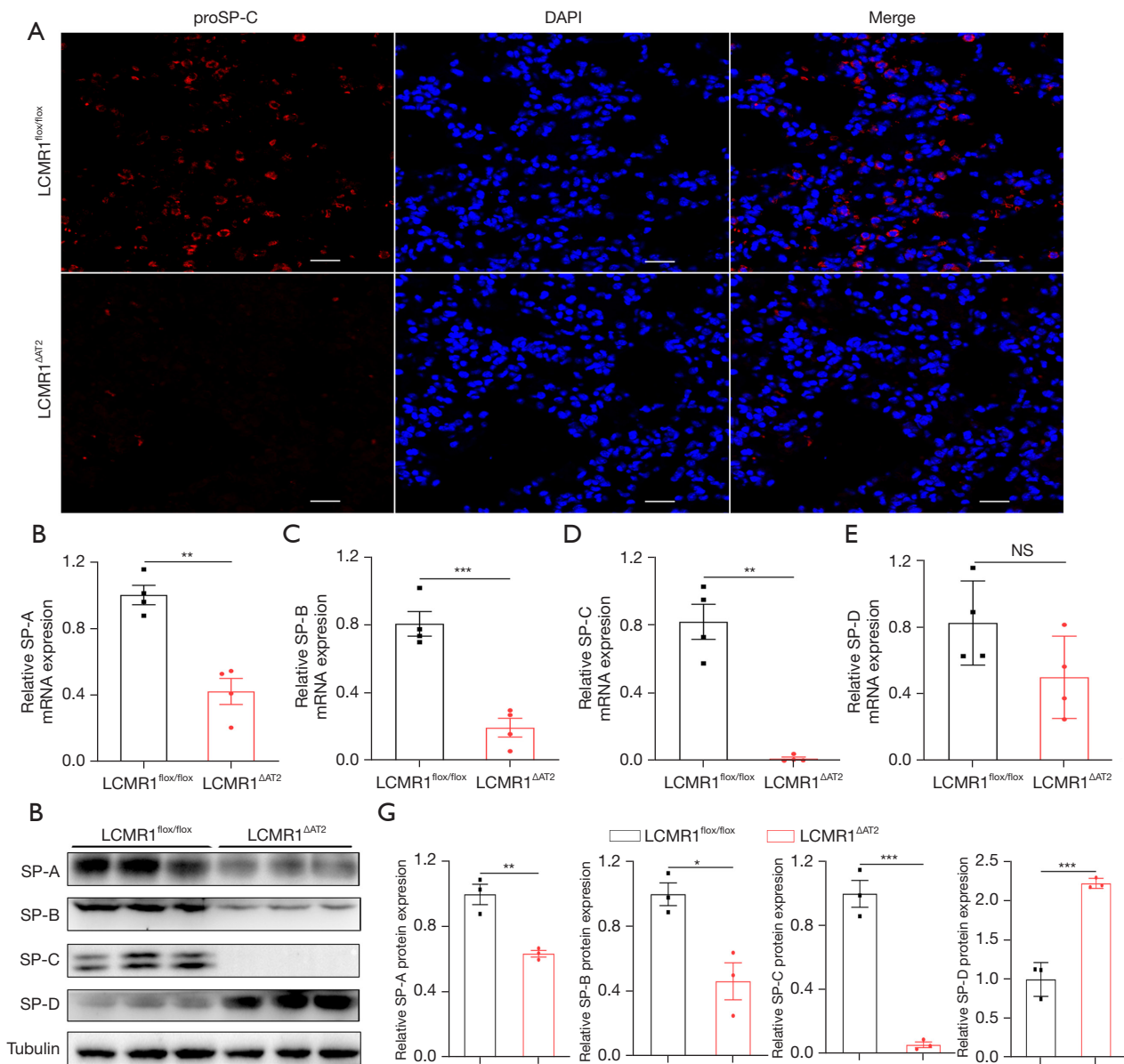


Figure 5 Effects of *LCMR1* deletion on the AT2 cell number and pulmonary surfactant proteins. (A) Representative images of immunofluorescence staining for proSP-C (red) in lung sections from *LCMR1^{flox/flox}* and *LCMR1^{ΔAT2}* mice on day 14 after tamoxifen administration. The nuclei were stained with DAPI (blue). Scale bars, 50 μ m. (B-E) qPCR analysis of the mRNA expressions of SP-A (B), SP-B (C), SP-C (D), and SP-D (E) in the lung tissue from *LCMR1^{flox/flox}* and *LCMR1^{ΔAT2}* mice on day 14 after tamoxifen administration, normalized to β -actin (n=4/group). (F,G) Western blot (F) and quantitative analysis (G) of the protein expressions of SP-A, SP-B, SP-C, and SP-D in lung tissues from *LCMR1^{flox/flox}* and *LCMR1^{ΔAT2}* mice on day 14 after tamoxifen administration, normalized to α -tubulin (n=3/group). Data are presented as the mean \pm SEM. *, P<0.05, **, P<0.01, ***, P<0.001; NS, not significant by unpaired Student's *t*-test. AT2, alveolar type II; *LCMR1*, lung cancer metastasis-related protein 1; SEM, standard error of mean.

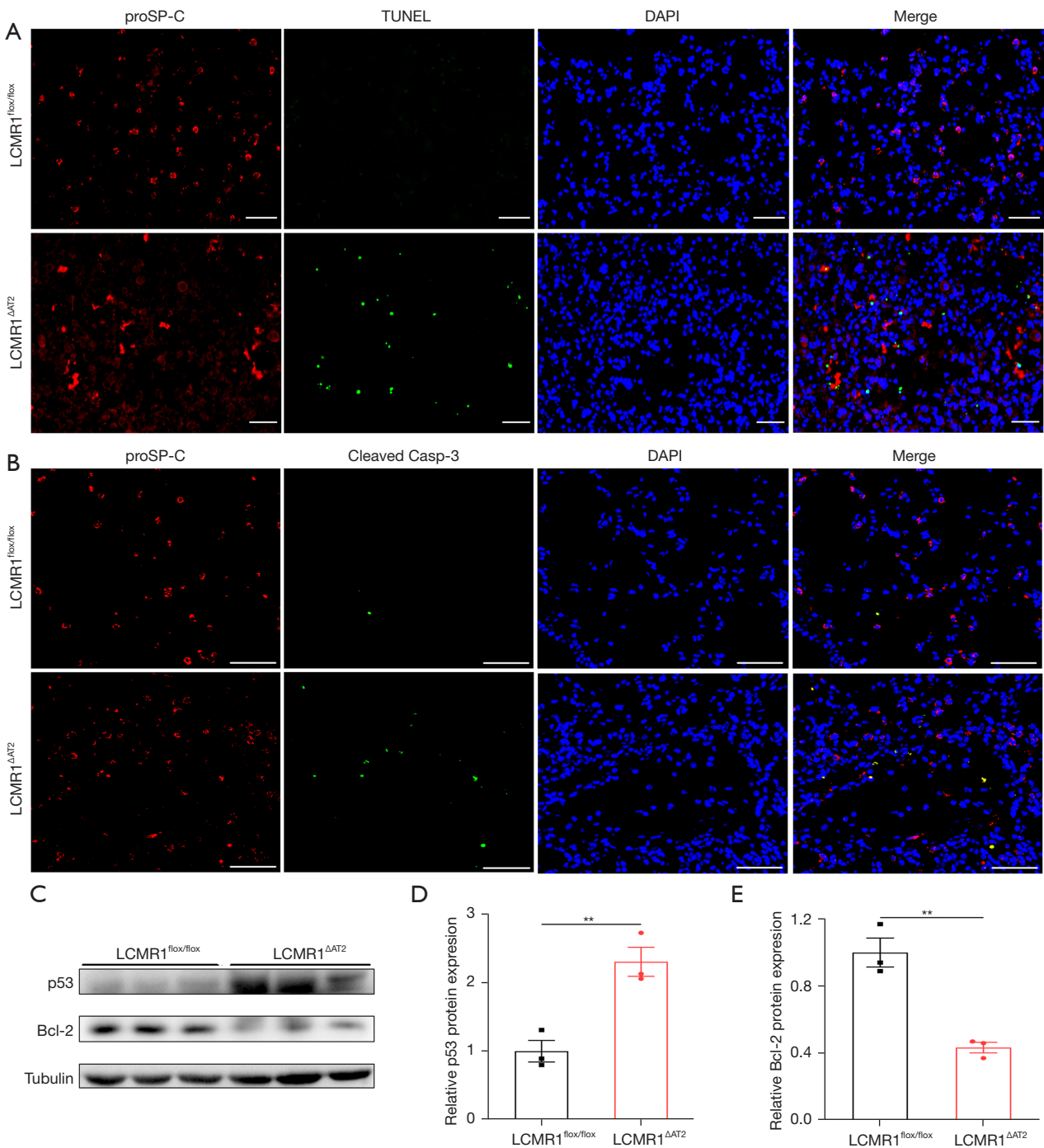


Figure 6 AT2 cell-specific *LCMR1* deletion promotes apoptosis in AT2 cells. (A) Representative images of proSP-C (red) and TUNEL (green) double staining of lung sections from *LCMR1*^{flox/flox} and *LCMR1*^{ΔAT2} mice on day 14 after tamoxifen administration. Nuclei were stained with DAPI (blue). Scale bars, 50 μm. (B) Representative images of proSP-C (red) and cleaved caspase-3 (green) double staining of lung sections from *LCMR1*^{flox/flox} and *LCMR1*^{ΔAT2} mice on day 10 after tamoxifen administration. Scale bars, 50 μm. (C-E) Western blot (C) and quantitative analysis of the protein expressions of p53 (D) and Bcl-2 (E) in AT2 cells from *LCMR1*^{flox/flox} and *LCMR1*^{ΔAT2} mice on day 14 after tamoxifen administration, normalized to β-actin (n=3/group). Data are presented as the mean ± SEM. **, P<0.01 by unpaired Student's *t*-test. AT2, alveolar type II; *LCMR1*, lung cancer metastasis-related protein 1; SEM, standard error of mean.

loxP system can efficiently act to direct tissue-specific, site-specific, and heritable chromosomal DNA recombination events in transgenic mice (32). Therefore, combining CRISPR/Cas9 and the Cre/loxP system makes it possible to precisely investigate gene functions in specific cells or tissues, which largely avoids the unspecific side effects of systemic gene knockdown (33). Additionally, with the fusion of Cre recombinase to the ligand-binding domain of estrogen receptor (Cre-ER), the deletion of floxed genes can be induced at the desired time by tamoxifen administration (34). Taking advantage of these sophisticated tools, we constructed a mouse strain carrying the conditional *LCMR1* allele with exons 2–4 flanked by loxP sites. We could achieve conditional gene inactivation of *LCMR1* in different tissue or cell types by crossing the *LCMR1*^{lox} mice with mice expressing specific Cre recombinase. In the present study, we bred *LCMR1*^{lox} mice with *Sftpc-CreER^{T2}* mice harboring tamoxifen-inducible Cre activity specifically in AT2 cells. To our knowledge, this is the first reported AT2 cell-specific *LCMR1* conditional knockout mouse model to date.

Surprisingly, all of the *LCMR1*^{ΔAT2} mice died within 17 days after tamoxifen administration in the absence of additional damaging agents, while all of the control mice were healthy and alive. We found massive AT2 cell loss in the lung tissues of *LCMR1*^{ΔAT2} mice through immunofluorescence staining for the AT2 cell marker, proSP-C. *LCMR1* knockdown was reported to promote cell apoptosis in human osteosarcoma, laryngocarcinoma, and lung cancer cells *in vitro* (2–4). In addition, adipose-specific *MED19* knockout in adult mice can cause lipodystrophy due to increased apoptosis and macrophage infiltration (12). Therefore, we hypothesized that AT2 cell loss in *LCMR1*^{ΔAT2} mice may be related to increased apoptosis. ProSP-C and TUNEL co-staining demonstrated more apoptotic AT2 cells in *LCMR1*^{ΔAT2} mice compared with those in *LCMR1*^{lox/lox} mice, as evidenced simultaneously by proSP-C and cleaved caspase-3 double staining. Furthermore, the elevated apoptosis in AT2 cells was confirmed by upregulated p53 protein and downregulated Bcl-2 protein expression. The regulation of AT2 cell apoptosis has been reported in some studies but the main molecular mechanism remains uncertain (35,36). Therefore, further research is needed to determine the specific molecular mechanism through which *LCMR1* deletion results in AT2 cell loss.

Here, we highlight two possible causes of death for *LCMR1*^{ΔAT2} mice. On the one hand, extensive AT2 cell loss resulting from *LCMR1* deletion destroyed the integrity of

the alveolar architecture, as evidenced by histopathological examinations. As essential components and stem cells of the alveolar epithelium, AT2 cells are important in alveolar maintenance and repair in the adult lung (14). Targeted injury of AT2 cells at a high level can cause lung injury, fibrosis, and even death in mice (37,38). On the other hand, the depletion of AT2 cells may also disrupt the homeostasis of pulmonary surfactant and weaken its function to lower the surface tension at the air-liquid interface. Despite the quantitative reduction of AT2 cells, we found dysmorphic or electron-dense lamellar bodies in AT2 cells through TEM, which may aggravate pulmonary surfactant dysfunction as lamellar bodies are functionally specialized organelles synthesizing and storing pulmonary surfactants in AT2 cells. SP-B and SP-C are the critical surfactant proteins involved in surfactant organization and its surface-active properties (39). We found significantly reduced expression of SP-B and SP-C in the lung tissues of *LCMR1*^{ΔAT2} mice compared with that of *LCMR1*^{lox/lox} mice, especially SP-C, which was almost undetectable. Nevertheless, the expression of SP-D was significantly increased in the lung tissues of *LCMR1*^{ΔAT2} mice. One possible cause may be that AT2 cells are not the only source of SP-D which can also be synthesized and secreted by Clara cells and macrophages (40). Additionally, the changes in histopathology, permeability, and the inflammatory response observed in the lung tissues of *LCMR1*^{ΔAT2} mice produced a phenotype with features resembling lung injury. It was previously reported that SP-D expression was increased in the lung tissues of animals with acute lung injury (41,42).

Conclusions

In conclusion, this study demonstrated for the first time that the conditional knockout of *LCMR1* specifically in the AT2 cells of adult mice results in a lethal phenotype with impaired lung structure and function. The main causes for this could lie in extensive AT2 cell loss, alveolar integrity destruction, and pulmonary surfactant deficiency. Our data indicate that *LCMR1* is essential for AT2 cell integrity and maintenance. These findings also highlight the critical role of AT2 cells in maintaining lung homeostasis.

Acknowledgments

We thank the Center for Biological Imaging, Institute of Biophysics, Chinese Academy of Science for assistance with transmission electron microscopy.

Funding: This work was supported by the National Natural Science Foundation of China (Nos. 30070335 and 30370616) and the China Postdoctoral Science Foundation (No. 20090461438).

Footnote

Reporting Checklist: The authors have completed the ARRIVE reporting checklist. Available at <https://jtd.amegroups.com/article/view/10.21037/jtd-23-293/rc>

Data Sharing Statement: Available at <https://jtd.amegroups.com/article/view/10.21037/jtd-23-293/dss>

Peer Review File: Available at <https://jtd.amegroups.com/article/view/10.21037/jtd-23-293/prf>

Conflicts of Interest: All authors have completed the ICMJE uniform disclosure form (available at <https://jtd.amegroups.com/article/view/10.21037/jtd-23-293/coif>). The authors have no conflicts of interest to declare.

Ethical Statement: The authors are accountable for all aspects of the work in ensuring that questions related to the accuracy or integrity of any part of the work are appropriately investigated and resolved. All animal experiments performed in this study were approved by the Institutional Animal Care Use Committee of Chinese PLA General Hospital (No. 2018-X14-25), in compliance with institutional guidelines for the care and use of animals.

Open Access Statement: This is an Open Access article distributed in accordance with the Creative Commons Attribution-NonCommercial-NoDerivs 4.0 International License (CC BY-NC-ND 4.0), which permits the non-commercial replication and distribution of the article with the strict proviso that no changes or edits are made and the original work is properly cited (including links to both the formal publication through the relevant DOI and the license). See: <https://creativecommons.org/licenses/by-nc-nd/4.0/>.

References

- Chen L, Liang Z, Tian Q, et al. Overexpression of *LCMR1* is significantly associated with clinical stage in human NSCLC. *J Exp Clin Cancer Res* 2011;30:18.
- Xu Y, Li C, Tian Q, et al. Suppression of lung cancer metastasis-related protein 1 promotes apoptosis in lung cancer cells. *Int J Mol Med* 2012;30:1481-6.
- Yu W, Zhang Z, Min D, et al. Mediator of RNA polymerase II transcription subunit 19 promotes osteosarcoma growth and metastasis and associates with prognosis. *Eur J Cancer* 2014;50:1125-36.
- Zhao Y, Meng Q, Gao X, et al. Down-regulation of mediator complex subunit 19 (Med19) induces apoptosis in human laryngocarcinoma HEP2 cells in an Apaf-1-dependent pathway. *Am J Transl Res* 2017;9:755-61.
- Sato S, Tomomori-Sato C, Parmely TJ, et al. A set of consensus mammalian mediator subunits identified by multidimensional protein identification technology. *Mol Cell* 2004;14:685-91.
- Boube M, Joulia L, Cribbs DL, et al. Evidence for a mediator of RNA polymerase II transcriptional regulation conserved from yeast to man. *Cell* 2002;110:143-51.
- Richter WF, Nayak S, Iwasa J, et al. The Mediator complex as a master regulator of transcription by RNA polymerase II. *Nat Rev Mol Cell Biol* 2022;23:732-49.
- Malik S, Roeder RG. The metazoan Mediator co-activator complex as an integrative hub for transcriptional regulation. *Nat Rev Genet* 2010;11:761-72.
- Soutourina J. Transcription regulation by the Mediator complex. *Nat Rev Mol Cell Biol* 2018;19:262-74.
- Dean JM, He A, Tan M, et al. MED19 Regulates Adipogenesis and Maintenance of White Adipose Tissue Mass by Mediating PPAR γ -Dependent Gene Expression. *Cell Rep* 2020;33:108228.
- Immarigeon C, Bernat-Fabre S, Guillou E, et al. Mediator complex subunit Med19 binds directly GATA transcription factors and is required with Med1 for GATA-driven gene regulation in vivo. *J Biol Chem* 2020;295:13617-29.
- Ding N, Tomomori-Sato C, Sato S, et al. MED19 and MED26 are synergistic functional targets of the RE1 silencing transcription factor in epigenetic silencing of neuronal gene expression. *J Biol Chem* 2009;284:2648-56.
- Rock JR, Barkauskas CE, Crouce MJ, et al. Multiple stromal populations contribute to pulmonary fibrosis without evidence for epithelial to mesenchymal transition. *Proc Natl Acad Sci U S A* 2011;108:E1475-83.
- Barkauskas CE, Crouce MJ, Rackley CR, et al. Type 2 alveolar cells are stem cells in adult lung. *J Clin Invest* 2013;123:3025-36.
- Chen Q, Liu Y. Heterogeneous groups of alveolar type II cells in lung homeostasis and repair. *Am J Physiol Cell Physiol* 2020;319:C991-C996.
- Basil MC, Katzen J, Engler AE, et al. The Cellular and Physiological Basis for Lung Repair and Regeneration: Past,

- Present, and Future. *Cell Stem Cell* 2020;26:482-502.
17. D'Agnillo F, Walters KA, Xiao Y, et al. Lung epithelial and endothelial damage, loss of tissue repair, inhibition of fibrinolysis, and cellular senescence in fatal COVID-19. *Sci Transl Med* 2021;13:eabj7790.
 18. Lechner AJ, Driver IH, Lee J, et al. Recruited Monocytes and Type 2 Immunity Promote Lung Regeneration following Pneumonectomy. *Cell Stem Cell* 2017;21:120-134.e7.
 19. Li FJ, Surolia R, Li H, et al. Citrullinated vimentin mediates development and progression of lung fibrosis. *Sci Transl Med* 2021;13:eaba2927.
 20. Gerard L, Lecocq M, Bouzin C, et al. Increased Angiotensin-Converting Enzyme 2 and Loss of Alveolar Type II Cells in COVID-19-related Acute Respiratory Distress Syndrome. *Am J Respir Crit Care Med* 2021;204:1024-34.
 21. Aga esse G, Barbolat-Boutrand L, Sulpice E, et al. A large-scale RNAi screen identifies LCMR1 as a critical regulator of α -melanocyte-stimulating hormone-mediated melanoma invasion. *Oncogene* 2017;36:446-57.
 22. Zhang X, Gao D, Fang K, et al. MED19 is targeted by miR-101-3p/miR-422a and promotes breast cancer progression by regulating the EGFR/MEK/ERK signaling pathway. *Cancer Lett* 2019;444:105-15.
 23. Wang K, Wang X, Fu X, et al. Lung cancer metastasis-related protein 1 promotes the transferring from advanced metastatic prostate cancer to castration-resistant prostate cancer by activating the glucocorticoid receptor α signal pathway. *Bioengineered* 2022;13:5373-85.
 24. Zhang Y, Qin P, Xu X, et al. Mediator Complex Subunit 19 Promotes the Development of Hepatocellular Carcinoma by Regulating the AKT/mTOR Signaling Pathway. *Front Oncol* 2021;11:792285.
 25. Zhang X, Wu J, Hu C, et al. CXCL11 negatively regulated by MED19 favours antitumour immune infiltration in breast cancer. *Cytokine* 2022;162:156106.
 26. Mali P, Yang L, Esvelt KM, et al. RNA-guided human genome engineering via Cas9. *Science* 2013;339:823-6.
 27. Knott GJ, Doudna JA. CRISPR-Cas guides the future of genetic engineering. *Science* 2018;361:866-9.
 28. Bai Y, Liu Y, Su Z, et al. Gene editing as a promising approach for respiratory diseases. *J Med Genet* 2018;55:143-149.
 29. Moses C, Kaur P. Applications of CRISPR systems in respiratory health: Entering a new 'red pen' era in genome editing. *Respirology* 2019;24:628-637.
 30. Sreedurgalakshmi K, Srikar R, Rajkumari R. CRISPR-Cas deployment in non-small cell lung cancer for target screening, validations, and discoveries. *Cancer Gene Ther* 2021;28:566-580.
 31. Liu X, Zhao X, Yuan Y, et al. Accurate detection of lung cancer-related microRNA through CRISPR/Cas9-assisted garland rolling circle amplification. *J Thorac Dis* 2022;14:4427-4434.
 32. Orban PC, Chui D, Marth JD. Tissue- and site-specific DNA recombination in transgenic mice. *Proc Natl Acad Sci U S A* 1992;89:6861-5.
 33. Liu B, Jing Z, Zhang X, et al. Large-scale multiplexed mosaic CRISPR perturbation in the whole organism. *Cell* 2022;185:3008-3024.e16.
 34. Feil R, Brocard J, Mascrez B, et al. Ligand-activated site-specific recombination in mice. *Proc Natl Acad Sci U S A* 1996;93:10887-90.
 35. Olajuyin AM, Zhang X, Ji HL. Alveolar type 2 progenitor cells for lung injury repair. *Cell Death Discov* 2019;5:63.
 36. Zheng J, Zhu S, Xu H, et al. miR-363-3p inhibits rat lung alveolar type II cell proliferation by downregulating STRA6 expression and induces cell apoptosis via cellular oxidative stress and G1-phase cell cycle arrest. *Transl Pediatr* 2021;10:2095-2105.
 37. Garcia O, Hiatt MJ, Lundin A, et al. Targeted Type 2 Alveolar Cell Depletion. A Dynamic Functional Model for Lung Injury Repair. *Am J Respir Cell Mol Biol* 2016;54:319-30.
 38. Sisson TH, Mendez M, Choi K, et al. Targeted injury of type II alveolar epithelial cells induces pulmonary fibrosis. *Am J Respir Crit Care Med* 2010;181:254-63.
 39. Milad N, Morissette MC. Revisiting the role of pulmonary surfactant in chronic inflammatory lung diseases and environmental exposure. *Eur Respir Rev* 2021;30:210077.
 40. Voorhout WF, Veenendaal T, Kuroki Y, et al. Immunocytochemical localization of surfactant protein D (SP-D) in type II cells, Clara cells, and alveolar macrophages of rat lung. *J Histochem Cytochem* 1992;40:1589-97.
 41. Sakamoto K, Hashimoto N, Kondoh Y, et al. Differential modulation of surfactant protein D under acute and persistent hypoxia in acute lung injury. *Am J Physiol Lung Cell Mol Physiol* 2012;303:L43-53.
 42. Yan XX, Zheng AD, Zhang ZE, et al. Protective effect of pantoprazole against sepsis-induced acute lung and kidney injury in rats. *Am J Transl Res* 2019;11:5197-211.
- (English Language Editor: J. Gray)

Cite this article as: Wang Y, Li C, Wu Z, Dai Y, Liu L, Chen L. Deletion of *LCMR1* in alveolar type II cells induces lethal impairment of lung structure and function in adult mice. *J Thorac Dis* 2023;15(3):1445-1459. doi: 10.21037/jtd-23-293

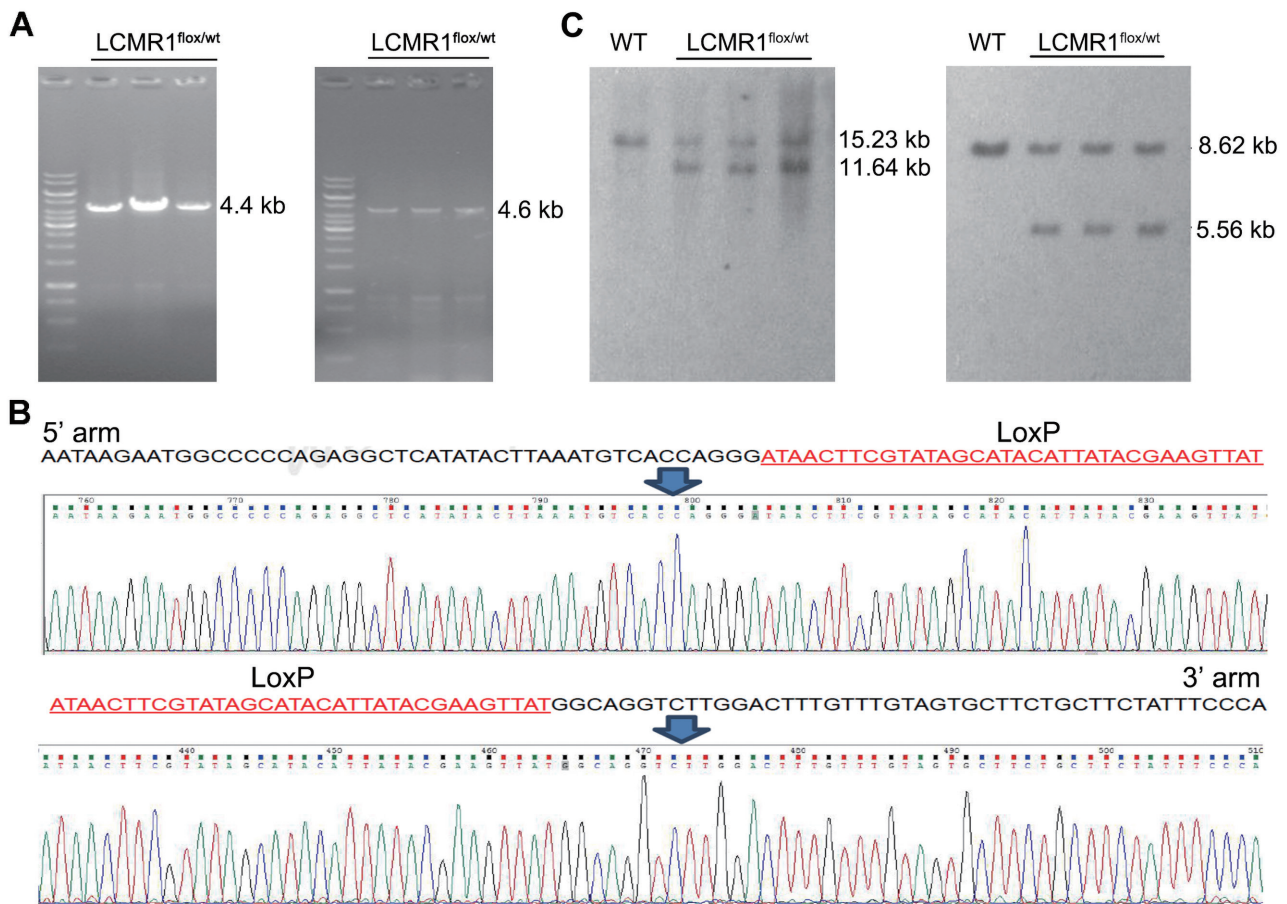


Figure S1 Identification and confirmation of the floxed *LCMR1* allele. (A) Representative agarose gel electrophoresis image of the PCR product amplified for genotyping. *LCMR1^{flox/wt}* mice exhibited 4.4-kb (left panel) and 4.6-kb bands (right panel) produced by the floxed *LCMR1* allele. (B) Sanger sequencing result of the above PCR products from a *LCMR1^{flox/wt}* mouse. (C) Southern blot analysis confirmed the correct insertion of the two loxP sites. The expected fragment size of gDNA hybridized with the 5' Probe (left panel): 15.23 kb (WT) and 11.64 kb (floxed allele); 3' Probe (right panel): 8.62 kb (WT) and 5.56 kb (floxed allele). Wt, wide type. PCR, polymerase chain reaction.

Table S1 Primers for PCR

Primer sequence	Product size, bp
LCMR1 ^{flox} (5'-loxP site) Forward: CACTGCCTCCCAAGTGAGTGCTG Reverse: CCCCAATGACCACACATAATCCTTC	Flox (265)/WT (198)
LCMR1 ^{flox} (3'-loxP site) Forward: ACATGAGTGCAGTATCCTGAGGC Reverse: AAATAGAAGCAGAAGCACTACAAAC	Flox (289)/WT (214)
LCMR1 ^{ΔAT2} Forward: CACTGCCTCCCAAGTGAGTGCTG Reverse: AAATAGAAGCAGAAGCACTACAAAC	Knockout (192)
Sftpc-CreER ^{T2} Forward: TGCTTCACAGGGTCCGGTAG Reverse 1: ACACCGCCTTATTCCAAG Reverse 2: CATTACCTGGGGTAGGACCA	Cre (210)/WT (327)

Table S2 Primers for quantitative RT-PCR

Gene	Forward primer	Reverse primer
<i>LCMR1</i>	CGATCCCTCATTGAGAAGCCT	TATGCATCAGACGACACTGCTC
<i>SP-A</i>	CTGTCCCAAGGAATCCAGAG	CCGTCTGAGTAGCGGAAGTC
<i>SP-B</i>	TGTGCCAAGAGTGTGAGGAT	CAGGGGCAGGTAGACATCAA
<i>SP-C</i>	ACATGAGTGCAGTATCCTGAGGC	AAATAGAAGCAGAAGCACTACAAAC
<i>SP-D</i>	AAGGTCCACGGGGTGAGAA	TTTGCCTTGAGGTCCTATGTTC
<i>β-actin</i>	CCTGGGCATGGAGTCCTGTG	TCTTCATTGTGCTGGGTGCC